




Article

Actuator FDI Scheme for a Wind Turbine Benchmark Using Sliding Mode Observers

Vicente Borja-Jaimes ¹, Manuel Adam-Medina ^{1,*}, Jarniel García-Morales ¹,
Gerardo Vicente Guerrero-Ramírez ¹, Betty Yolanda López-Zapata ² and Eduardo Mael Sánchez-Coronado ³

¹ Electronic Engineering Department, TecNm/National Center for Research and Technological Development (CENIDET), Cuernavaca, Morelos 62490, Mexico; vicentebj@cenidet.edu.mx (V.B.-J.); jarniel.gm@cenidet.tecnm.mx (J.G.-M.); gerardo.gr@cenidet.tecnm.mx (G.V.G.-R.)

² Department of Mechatronic Engineering, Polytechnic University of Chiapas, Tuxtla Gutierrez, Chiapas 29082, Mexico; blopez@upchiapas.edu.mx

³ Department of Mechatronic Engineering, Technological University of the Center of Veracruz, Cuitlahuac, Veracruz 94910, Mexico; eduardo.sanchez@utcv.edu.mx

* Correspondence: manuel.am@cenidet.tecnm.mx

Abstract: This paper proposes a fault detection and isolation (FDI) scheme for a wind turbines subject to actuator faults in both the pitch system and the drive train system. The proposed scheme addresses fault detection and isolation problems using a fault estimation approach. The proposed approach considers the use of a particular class of sliding mode observers (SMOs) designed to maintain the sliding motion even in the presence of actuator faults. The fault detection problem is solved by reconstructing the actuator faults through an appropriate analysis of the nonlinear output error injection signal, which is required to keep the SMO in a sliding motion. To ensure accurate fault reconstruction, only two conditions are required, namely that the faults are bounded and they meet the matching condition. A scheme based on a bank of SMOs is proposed to solve the fault detection and isolation problem in the pitch system. For the drive train system, a scheme using only one SMO is proposed. The performance of the proposed FDI scheme is validated by using a wind turbine benchmark model subjected to several actuator faults. Normalized root mean square error (NRMSE) analysis is performed to evaluate the accuracy of the actuator fault estimations.

Keywords: fault detection and isolation (FDI); sliding mode observer (SMO); wind turbines



Citation: Borja-Jaimes, V.; Adam-Medina, M.; García-Morales, J.; Guerrero-Ramírez, G.V.; López-Zapata, B.Y.; Sánchez-Coronado, E.M. Actuator FDI Scheme for a Wind Turbine Benchmark Using Sliding Mode Observers. *Processes* **2023**, *11*, 1690. <https://doi.org/10.3390/pr11061690>

Academic Editors: Francisco Ronay López-Estrada and Guillermo Valencia-Palomo

Received: 18 April 2023
Revised: 21 May 2023
Accepted: 25 May 2023
Published: 1 June 2023



Copyright: © 2023 by the authors. Licensee MDPI, Basel, Switzerland. This article is an open access article distributed under the terms and conditions of the Creative Commons Attribution (CC BY) license (<https://creativecommons.org/licenses/by/4.0/>).

1. Introduction

Nowadays, wind turbines contribute a large part of the world's electrical energy production from renewable sources. In 2022, their second-highest growth in history was registered, with 93.6 GW of installed capacity added, which is only 1.8% below the historical record reached in 2020. The addition in 2022 carries the global cumulative installed capacity of wind energy to 837 GW, which, on average, represents a growth of 12% per year [1]. The remarkable growth that wind turbines have experienced has led to a growing demand for greater efficiency and reliability. However, the size, the complexity of the components, and the stochastic behavior of the wind present significant challenges when trying to maintain an operation with a preset efficiency [2]. Furthermore, wind turbines, like any complex system, are susceptible to faults. Various factors including environmental factors, manufacturing defects, and lack of maintenance can cause wind turbine faults, leading to significant damage and operational disruptions. Additionally, wind turbines are installed in remote and isolated locations, which complicates preventive and corrective maintenance actions, whereby the incidence of a fault can trigger breakdowns or even the destruction of the turbine if it is not detected [3]. This situation has generated interest in the application of fault detection and isolation (FDI) methods in wind turbines, especially in critical wind turbine components such as the pitch and drive train systems [4].

FDI is crucial for ensuring the reliable and safe operation of wind turbines. The primary objective of an FDI scheme is to generate a warning when an unusual situation occurs in the operation of the system and then to find its source and location [5]. Overviews and surveys of FDI methods for wind turbines appear in [6–9]. Most of the works reported in the literature can be divided into two large groups: data-driven and model-based methods. Many data-driven techniques have been developed to detect faults in wind turbines based on fuzzy systems and neural networks [10], kernel methods [11], deep neural networks (DNN) and principal component analysis (PCA) [12], classifier fusion [13], and condition monitoring systems [14]. Of these data-driven approaches, condition monitoring systems are the most effective because they provide substantial information about irregularities in the system. However, one drawback of most condition monitoring methods is the slow and tedious data collection and interpretation.

Model-based FDI methods utilize mathematical models of the wind turbine system to simulate its behavior under normal and faulty conditions. These methods rely on comparing the model predictions with sensor measurements to detect and isolate faults [15]. One of the most common methods of model-based FDI schemes is the observer-based method. This method involves designing observers, also known as estimators or filters, to estimate the internal states of the wind turbine based on signals measured by sensors. By comparing the estimated states with the measured states, deviations can be detected and attributed to specific faults [16]. Many observer-based FDI schemes have been developed for wind turbines. In [17], an adaptive observer FDI scheme is proposed. The observer is used to estimate both sensor and actuator faults in the benchmark model proposed in [18]. An algorithm for detecting pitch actuator faults using interval observers is proposed in [19]. The algorithm is trained with healthy parameters of the system, and it is assumed that in the presence of faults, the values of the parameters do not stray too far from their fault-free condition, which is unrealistic. A model-based FDI scheme for the pitch system was proposed in [20]. The scheme uses an extended Kalman filter to detect faults. The Kalman filter applies multiple model-adaptive estimators to approximate the states of the pitch system. A scheme to detect both actuator and sensor faults in a wind turbine benchmark model based on an unknown input observer is proposed in [21]. For fault detection, it employs residual signals; for fault isolation, it utilizes estimating states, output signals, and control signals.

The vast majority of proposed FDI schemes for both sensor and actuator faults in wind turbines use a residual generation approach. In a residual-based approach, residuals are ideally expected to be zero during fault-free operation and non-zero in a failed operation [22]. However, since a wind turbine is subject to disturbances, parameter uncertainty, and mismatches between the mathematical model and the actual system, these discrepancies can produce non-zero residuals even in a fault-free operation, creating a false alarm problem. The false alarms can affect FDI performance to such an extent that it may become useless. To overcome these difficulties, the model-based FDI scheme must be made insensitive to modeling uncertainty but sensitive to faults, which is called a robust FDI scheme [23].

A robust FDI scheme is proposed in [24]. The scheme considers actuator and sensor faults in both the pitch and drive train systems. Robustness is achieved by decoupling the faulty dynamics from the system using coordinate transformations.

Sliding mode techniques have historically demonstrated robustness properties for a certain class of matched uncertainties [25]. In particular, sliding mode observers (SMOs) have been used for both fault detection and isolation as well as fault-tolerant control (FTC) schemes [26]. Alternatives to taking advantage of the inherent robustness of the SMO for fault detection and isolation problems have been explored in wind turbines. A model-based FDI scheme for simultaneously detecting sensor and actuator faults is presented in [27]. The proposed scheme uses an adaptive SMO to accurately estimate both system states and disturbances as part of an active FTC system. An FDI scheme using SMOs is designed in [28]. The SMOs are combined with a residual signal generator for detecting sensor faults in both the pitch and drive train systems in a wind turbine benchmark model. The

proposed schemes require the designer to know the behavior of the fault to establish an adequate threshold to be able to perform fault detection. However, this is an impractical approach since fault behavior is continually changing [29]. Thus, an FDI scheme using an observer-based approach can only detect faults considered in the fault propagation analysis of the system for which a detection threshold is established. Recently, fault diagnosis methods that not only detect and isolate faults but are also capable of making a complete estimate of faults have attracted great interest. Complete fault information is crucial to an FTC system that can effectively mitigate fault effects, enabling the wind turbine to operate safely and with reduced downtime [30]. A fault estimation approach using adaptive and parameter estimation schemes for a wind turbine is proposed in [31]. The parameter estimation scheme is utilized to estimate the values of specific parameters that may be affected by faults or abnormalities in the wind turbine. A robust actuator multiplicative fault estimation method with unknown input decoupling is presented in [32]. The method employs a multiplicative fault model and an unknown input decoupling technique to mitigate the influence of unknown inputs on the fault estimation process. Although some effective fault estimation techniques for wind turbines have been presented, most of them have focused on parametric faults, leaving the application of fault estimation techniques in critical components of the wind turbine, such as the pitch and drive train systems, as an unresolved issue.

This paper addresses the problem of designing an FDI scheme for actuator faults in the pitch and drive train systems of a wind turbine using a fault estimation approach. The proposed method can detect and isolate the source of actuator faults. In addition, it provides a complete reconstruction of the faults. Therefore, the fault estimation method provides a direct estimate of the size and severity of the faults, which can be crucial for FTC schemes.

The main contributions of this paper are as follows:

- An FDI scheme for both the pitch and drive train systems that does not require explicit information from the fault. The only fault information required is the fault to be bounded.
- In contrast to the works reported in [20,23], the proposed FDI scheme employs the concept of an equivalent output error injection term. This allows a complete reconstruction of actuator faults while providing accurate estimates of states, regardless of fault occurrence.
- A simple method for actuator fault reconstruction using a low-pass filter (LPF) that analyzes the so-called nonlinear output error injection, in contrast to the works presented in [20,23], which use more complex methods.

This paper is organized as follows. The wind turbine model, the design methodology of an SMO for actuator fault reconstruction, and the proposed actuator FDI scheme for both the pitch and the drive train systems are presented in the Section 2. Simulation results of the proposed FDI scheme are presented in the Section 3. A discussion of the results is presented in the Section 4. Finally, conclusions are presented in the Section 5.

2. Materials and Methods

2.1. Mathematical Model of the Wind Turbine

A wind turbine converts wind energy into electrical energy by using the aerodynamic force of the turbine rotor blades. The input to the system is the wind speed, which causes the rotation of the turbine blades. This motion spreads through the turbine rotor. The drive train couples this motion with the generator shaft. In turn, the generator is responsible for transforming mechanical energy into electrical energy. The electrical power generated by the system is controlled by modifying the aerodynamics of the turbine, adjusting the angle of inclination of the blades, or modifying the speed of rotation of the generator shaft. In any case, the objective of the control system is to maintain the required electrical power. Figure 1 shows the interconnection of different subsystems that make up a wind turbine and their interaction with the control used to regulate electrical power. This model addresses the wind turbine at a system level and provides mathematical models with simplicity and

sufficient accuracy for all subsystems. The variables associated with Figure 1 are defined as follows: v_ω is the wind speed, τ_r is the rotor torque, τ_g is the generator torque, ω_r is the rotor speed, ω_g is the generator speed, E_g is the electrical power, $\tau_{g,ref}$ is the reference torque of the generator, β is the pitch angle, and β_{ref} is the reference angle of the pitch.

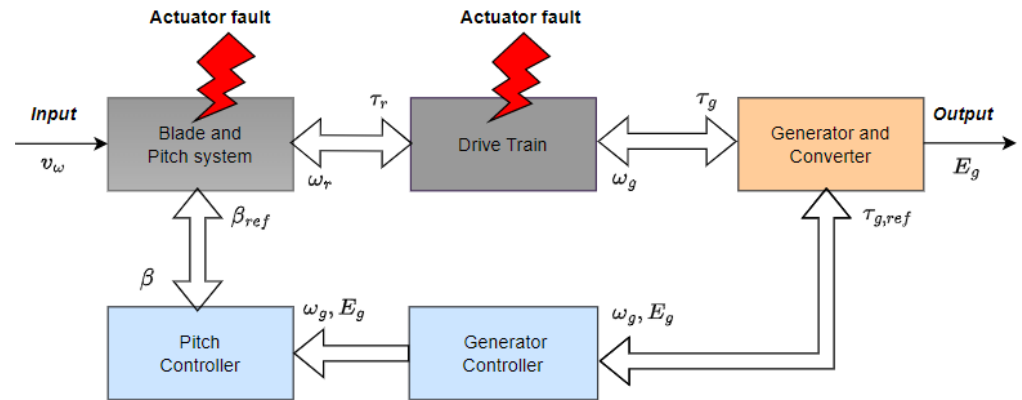


Figure 1. Wind turbine benchmark model.

For a more detailed description of the different subsystems of the wind turbine benchmark model and its internal connection, see [18]. The subsystems models are briefly described below.

2.1.1. Blade and Pitch Model

This system combines both aerodynamic and hydraulic pitch models. The wind turbine's nonlinear aerodynamic is modeled as a torque acting on the blades. The torque is given as

$$\tau_r(t) = \frac{1}{2} \pi \rho r^3 v_\omega^2(t) S(\lambda, \beta) \quad (1)$$

where $S(\lambda, \beta)$ represents a mapping of the coefficients, which depends on the tip speed ratio λ and the pitch angle β . r is the rotor ratio, ρ is the density of the air, and v_ω is the wind speed. Since the pitch system is composed of three identical subsystems its aerodynamics are stated as follows:

$$\tau_r(t) = \sum_{1 < i \leq 3} \frac{\pi \rho r^3 v_{\omega,i}^2(t) S(\lambda, \beta_i)}{6} \quad (2)$$

It is important to highlight that this model is valid for small differences between the pitch angles.

The hydraulic pitch system is modeled as a closed-loop second-order transfer function described as

$$\frac{\beta(s)}{\beta_{ref}(s)} = \frac{\psi^2}{s^2 + 2\zeta\psi s + \psi^2} \quad (3)$$

where β is the measurement pitch position angle and β_{ref} is the reference input provided by the wind turbine controller. ζ is the damping factor and ψ is the natural frequency.

2.1.2. Drive Train Model

The drive train system uses a simple two-mass model. Therefore, the nominal dynamics of the drive train system can be represented by

$$j_r \dot{\omega}_r(t) = \tau_r(t) - k_{dt} \theta(t) - (h_{dt} + b_r) \omega_r(t) + \frac{h_{dt}}{N_g} \omega_g(t) \quad (4)$$

$$j_g \dot{\omega}_g(t) = \frac{\eta_{dt} k_{dt}}{N_g} \theta(t) + \frac{\eta_{dt} h_{dt}}{N_g} \omega_r(t) - \left(\frac{\eta_{dt} h_{dt}}{N_g^2} + b_g \right) \omega_g(t) - \tau_g(t) \quad (5)$$

$$\dot{\theta}(t) = \omega_r(t) - \frac{1}{N_g} \omega_g(t) \quad (6)$$

where $\omega_r(t)$ and $\omega_g(t)$ are the rotor and generator speed and $\theta(t)$ denotes the torsion angle of the drive train system. The inputs $\tau_g(t)$ and $\tau_r(t)$, represent the torque of the rotor and generator, respectively. J_r and J_g are the moment of inertia of the low- and high-speed shafts, respectively. b_r and b_g are the viscous frictions of the low- and high-speed shafts, respectively. k_{dt} is the torsion stiffness of the drive train system, h_{dt} represents the torsion damping coefficient of the drive train, N_g is the gear ratio, and η_{dt} is the efficiency percentage of the drive train system.

2.1.3. Generator and Converter Model

The dynamics of the generator and converter can be modeled as a first-order transfer function because the frequency range used in the benchmark model is much smaller than the speed of the electrical subsystem and its controllers. The joint dynamics of the converter and generator are given by

$$\frac{\tau_g(s)}{\tau_{g,ref}(s)} = \frac{\gamma}{s + \gamma} \quad (7)$$

where $\tau_{g,ref}$ is the reference value and γ is the cutoff frequency. The electrical power produced by the generator is given by

$$E_g(t) = \eta_g \omega_g(t) \tau_g(t) \quad (8)$$

where E_g is the power produced by the generator and η_g is the efficiency of the generator.

2.1.4. Faults in Wind Turbines

In general, a fault refers to an error or defect in something that causes it to not work properly or function as intended [33]. In the context of wind turbines, a fault typically refers to a malfunction or failure in the wind turbine's components, systems, or operations that can lead to reduced performance, downtime, or even safety risks. The faults can occur in various parts of the wind turbine, including the pitch system, the drive train system, the generator, the electrical system, and the control system [34]. In addition, wind turbine faults can occur in both the actuators and sensors of any of the systems that make up the wind turbine. However, in this paper, we only focus on actuator faults in the pitch and the drive train systems.

According to a report published by the National Renewable Energy Laboratory (NREL) in the US, the most common faults in wind turbines include electrical system faults, blade damage, and mechanical faults [35]. Faults in wind turbines can have several consequences affecting the performance and safety of the wind turbine. Two critical components in the wind turbine are the pitch and the drive train systems. If a fault in any of these components is not detected on time, this can cause severe consequences for the wind turbine, such as reduced energy generation, increased downtime, higher maintenance and repair costs, and safety risks. Early detection and isolation in the pitch system as well as the drive train system are crucial for ensuring the optimal performance, reliability, and safety of the wind turbine [36]. Therefore, in this paper, we focus on the problem of fault detection and isolation in the pitch and drive train systems. It is worth noting that simultaneous faults in wind turbines can occur, although they are relatively rare. Accordingly, the case of simultaneous faults is not considered.

The severity of actuator faults in wind turbines can vary depending on the specific fault and its impact on the wind turbine's operation. Based on their severity, actuator faults are classified as abrupt, incipient, and intermittent faults. These actuator faults can be modeled using signal models that include the effect of the fault on the output of the actuator.

In normal wind turbine operation, the output of the actuator increases smoothly in response to the input. However, during an abrupt actuator fault, the output of the actuator

may experience sudden changes or fluctuations, leading to a non-smooth response. Hence, to model an abrupt actuator fault, a square signal model is used. In contrast, an incipient actuator fault in a wind turbine is a fault that is just beginning to develop, and its behavior is characterized by subtle changes in the actuator's output. Over time, the behavior of an incipient fault may become more pronounced, with the output of the actuator becoming increasingly irregular or unstable. Then, an incipient fault can be modeled using a time-varying signal model that allows for the characterization of the actuator's output over time [37]. Therefore, to simulate an incipient actuator fault, both sinusoidal and sawtooth signal models are proposed.

2.2. Design of Sliding Mode Observers for Actuator Fault Reconstruction

In recent years, SMOs have been successfully applied to solve the problem of estimating the states in dynamical systems. One of their most interesting properties, which has been used most in the literature, is robustness. This allows an SMO to successfully solve the estimation problem despite the presence of disturbances or uncertainties bounded within the system. In essence, an SMO is a mathematical replica of the system fitted by means of feedback of the output estimation error through a nonlinear function, which provides an interesting solution to this issue. The SMO can force the output estimation error to zero in finite time by determining the bound on the magnitude of the disturbance acting on the system. Consequently, the observer states converge asymptotically to the system states. Under this condition, it is said that a sliding motion takes place [38].

During the sliding motion, the nonlinear output estimation error contains information about unknown signals affecting the system. By suitably filtering the nonlinear output estimation error, unknown signals can be obtained. Therefore, by modeling faults as unknown signals, it is possible to use an SMO to reconstruct and, thus, detect and isolate these faults. The SMO design methodology is described below.

Consider the linear dynamical system subject to actuator faults described by

$$\dot{x}(t) = Fx(t) + Gu(t) + Mf_a(t, x, u) \quad (9)$$

$$y(t) = Hx(t) \quad (10)$$

where $F \in \mathbb{R}^{n \times n}$, $G \in \mathbb{R}^{n \times m}$, $H \in \mathbb{R}^{p \times n}$, and $M \in \mathbb{R}^{n \times q}$ with $p \geq q$. Assume that the matrices G , H , and M are the full rank, and the function $f_a : \mathbb{R}^+ \times \mathbb{R}^n \times \mathbb{R}^m \rightarrow \mathbb{R}^q$ is deemed to represent an actuator fault that is assumed to be bounded so that $\|f_a(t, x, u)\| \leq \alpha$ with $\alpha \in \mathbb{R}^+$.

In addition, consider that the dynamical system given in Equations (9) and (10) satisfies the following two conditions:

- $\text{rank}(HM) = q$;
- the invariant zeros of the system represented by the triple (F, G, H) must lie in \mathbb{C}^- .
- Under these conditions, there is a linear change of coordinates T , such that the new coordinate the system can be written as

$$\dot{x}_1(t) = F_{11}x_1(t) + F_{12}x_2(t) + G_1u(t) \quad (11)$$

$$\dot{x}_2(t) = F_{21}x_1(t) + F_{22}x_2(t) + G_2u(t) + M_2f_a(t, x, u) \quad (12)$$

$$y(t) = Cx(t) \quad (13)$$

where $x_1 \in \mathbb{R}^{n-p}$, $x_2 \in \mathbb{R}^p$, and F_{11} has stable eigenvalues. The coordinate system described above is used as a platform for the design of an SMO. The SMO structure that will be considered can be written in the form

$$\dot{\hat{x}}_1(t) = F_{11}\hat{x}_1(t) + F_{12}\hat{x}_2(t) + G_1u(t) - F_{12}e_y(t) \quad (14)$$

$$\dot{\hat{x}}_2(t) = F_{21}\hat{x}_1(t) + F_{22}\hat{x}_2(t) + G_2u(t) - (F_{22} - F_{22}^s)e_y(t) + w(t) \quad (15)$$

where F_{22}^s is a stable design matrix, and the discontinuous function $w(t)$ is defined as

$$w(t) = \begin{cases} -\sigma \|M_2\| \frac{P_2 e_y(t)}{\|P_2 e_y(t)\|} & \text{if } e_y(t) \neq 0 \\ 0 & \text{otherwise} \end{cases} \quad (16)$$

where $P_2 \in R^{p \times p}$ is a symmetric positive definite Lyapunov matrix for F_{22}^s . If the state estimation error and the output estimation errors are defined as $e_1(t) = \hat{x}_1(t) - x_1(t)$ and $e_y(t) = \hat{x}_2(t) - x_2(t)$, respectively, it is straightforward to show that the dynamical of the error is given by

$$\dot{e}_1(t) = F_{11}e_1(t) \quad (17)$$

$$\dot{e}_y(t) = F_{21}e_1(t) + F_{22}^s e_y(t) + w(t) - M_2 f_a(t, x, u) \quad (18)$$

It is shown by Edwards and Spurgeon in [38] that the dynamical of the error in Equations (17) and (18) is quadratically stable, and a sliding motion is achieved in finite time, forcing both $e_y(t)$ and $\dot{e}_y(t)$ to zero. Therefore, the dynamical system in Equations (14) and (15) can be considered as an SMO for the dynamical system in Equations (11)–(13). However, it is more convenient to express it in terms of the original coordinates system as

$$\dot{\hat{x}}(t) = Fx(t) + Gu(t) - K_l e_y(t) + K_{nl} w(t) \quad (19)$$

where K_l and K_{nl} are the linear and nonlinear gain matrices given by

$$K_l = T^{-1} \begin{bmatrix} F_{12} \\ F_{22} - F_{22}^s \end{bmatrix}, \quad (20)$$

and

$$K_{nl} = \|M_2\| T^{-1} \begin{bmatrix} 0 \\ I_p \end{bmatrix} \quad (21)$$

The output estimation error injection term, which is a nonlinear discontinuous signal, is defined as

$$w(t) = \begin{cases} -\sigma \|M_2\| \frac{P_2 H e_x(t)}{\|P_2 H e_x(t)\|} & \text{if } H e_x(t) \neq 0 \\ 0 & \text{otherwise} \end{cases} \quad (22)$$

where the state estimation error is defined as $e_x(t) = \hat{x}(t) - x(t)$ and the scalar σ is chosen so that $\sigma > \|f_a(t, x, u)\|$. It is important to note that even when the model considered for the design of the SMO has actuator fault signals, the dynamics of the observer do not depend on the faults. Therefore, the convergence of the observer is achieved even in the presence of actuator faults. The SMO design methodology described in this part is applied in the next subsection to develop an actuator FDI scheme for a wind turbine benchmark model.

2.3. Actuator FDI Scheme Based on Sliding Mode Observers

The traditional approach to FDI schemes using SMOs ensures that the sliding mode is interrupted when a fault occurs in the system, and the fault information is obtained by analyzing the residual signals. Under nominal fault-free conditions, the residuals are expected to be zero or nonzero when a fault occurs. In addition, most approaches that use residual generation can detect and isolate faults, but they do not provide information about the faults. In contrast to the traditional FDI methods, this paper addresses the fault detection and isolation problem by using a fault estimation approach based on the analysis of the nonlinear output error injection signal. One of the benefits of this approach compared to other SMOs based on FDI schemes is that the sliding motion is not broken, even when a

fault appears. This allows the use of the SMO as a state estimator and, most importantly, as an estimator of faults in the system.

Figure 2 shows the proposed architecture for actuator fault reconstruction using an SMO. The scheme is based on a mathematical model of the system, which describes the dynamics of the plant, actuators, and sensors. The model includes the fault description in the actuator, which is modeled as an additive signal. Then, an SMO is designed to achieve asymptotic convergence of the estimation error to zero. The SMO uses the plant outputs, inputs, and the difference between the system's outputs and the observer's outputs, named output estimation error. The output estimation error signal is fed back into the observer via a nonlinear function, which provides two advantages. Firstly, the SMO can force the output estimation error to zero in finite time, even in the presence of actuator faults acting in the system. This is possible because the nonlinear output error injection signal compensates for the effect of actuator faults throughout the system to maintain the sliding motion. Therefore, the observer states converge asymptotically to the system states.

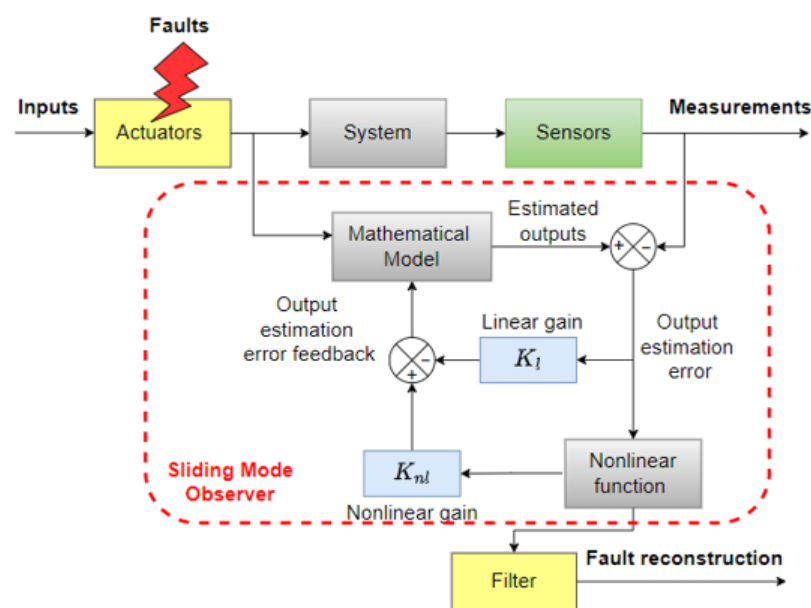


Figure 2. Actuator FDI scheme based on a sliding mode observer.

Secondly, once the output estimation error is forced to zero, it is said that a sliding motion takes place. During the sliding movement, the nonlinear output estimation signal injected into the SMO contains information about the faults affecting the system actuator. Then, by applying a suitable filtering process to the nonlinear output estimation error, the actuator fault can be reconstructed.

The idea behind this approach is to take advantage of the properties of the sliding motion and use the nonlinear output estimation error injection signal to reconstruct the actuator faults. Once a sliding motion is attained, $e_y(t) = 0$ and $\dot{e}_y(t) = 0$ are forced to zero in finite time, so the dynamics of the output estimation error in Equations (17) and (18) can be written as

$$0 = F_{21}e_1(t) + w(t) - M_2f_a(t, x, u) \quad (23)$$

Given that F_{11} is stable, it follows that $e_1(t) \rightarrow 0$ and, therefore, $w(t) = M_2f_a(t, x, u)$. That is, the fault information is contained in the nonlinear injection signal $w(t)$. Since the signal $w(t)$ switches at a very high frequency, one way to estimate the actuator fault is using a low-pass filter (LPF). The key point here is that to achieve a sliding motion in the presence of faults, it is only required that the magnitude of the fault is bounded and that it meets the matching condition, namely that the fault lies within the range space of the input distribution matrix of the system. However, the sliding motion cannot be maintained if the

condition $\sigma > \|f_a(t, x, u)\|$ is not satisfied for $t_0 > 0$, where t_0 represents the time at which the sliding motion is achieved.

2.3.1. Actuator FDI Scheme for the Pitch System

The pitch actuator is an important component of a wind turbine and is responsible for controlling the position and orientation of the turbine blades to optimize energy capture and maintain safe operation. If a fault in the pitch actuator is not detected on time, it can have serious consequences for the safe and efficient operation of the wind turbine.

For example, a pitch actuator fault can cause the turbine blades to become misaligned. This can cause stress and damage to other components of the turbine, such as the drive train and the generator. Over time, this can lead to more serious damage and the need for costly repairs or replacements.

There are several potential causes for pitch actuator faults, which can be classified into external (environmental factors) and internal causes. Environmental factors, such as exposure to wind, rain, and saltwater, can cause corrosion, erosion, or damage to actuator components. On the other hand, the internal sources of pitch actuator faults are the hydraulic system and the electrical motor in charge of turbine blade movement. For example, wiring issues or power surges can cause damage to the electrical components of the actuator, while hydraulic fluid leaks or clogs can impair the function of hydraulic actuators [39].

Figure 3 shows the proposed architecture for actuator fault detection and isolation in the pitch system. The proposed scheme consists of a bank of three SMOs to estimate the outputs of each of the three pitch subsystems. As each pitch subsystem is independent of the others, one observer receives only the input u_{pb} and output y_{pb} signals from a single pitch subsystem, that is, the observer is sensitive only to the faults of the monitored pitch subsystem, which ensures a solution to the fault isolation problem once a fault is detected.

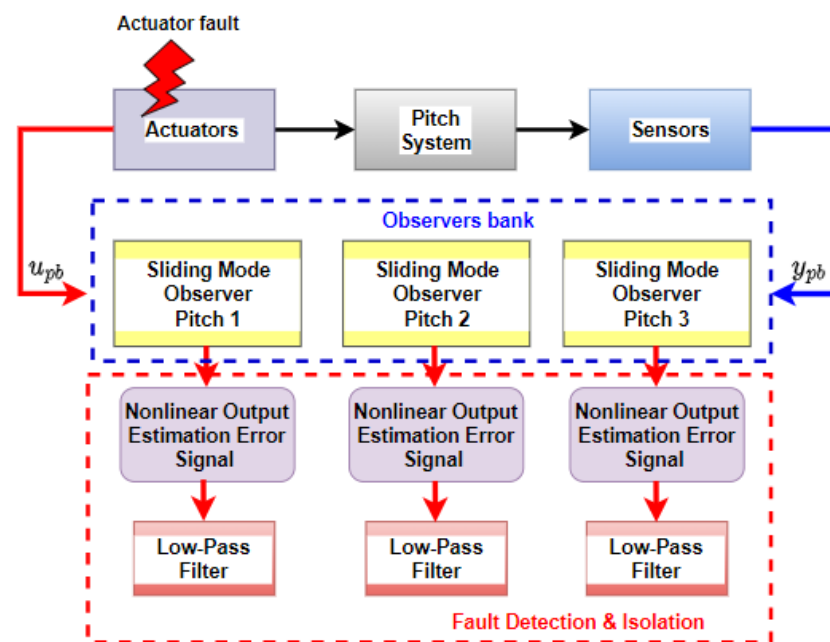


Figure 3. Actuator FDI scheme for the pitch system.

Since the nonlinear output estimation error injection signal compensates for the effect of faults in the SMO in order to maintain the sliding motion, fault detection is performed through the reconstruction of fault signals by filtering the nonlinear output error injection signal of each pitch subsystem.

As the pitch system is composed of three independent and identical subsystems, the SMO design presented in this section is applied identically to the other two subsystems.

The design of the SMO for one of the pitch subsystems considers the state space model given by

$$\dot{x}_{pb}(t) = F_{pb}x_p(t) + G_{pb}u_{pb}(t) + M_{pb}f_a(t) \quad (24)$$

$$y_{pb}(t) = H_{pb}x_{pb}(t) \quad (25)$$

where $x_{pb} \in \mathbb{R}^2$ is the state vector, $y_{pb} \in \mathbb{R}^2$ is the output vector, $u_{pb} \in \mathbb{R}$ is the input vector, $f_a(t)$ is any actuator fault signal, in this case of one dimension, and the matrices F_{pb} , G_{pb} and H_{pb} are defined as follows:

$$F_{pb} = \begin{bmatrix} 0 & 1 \\ -\psi^2 & -2\zeta\psi \end{bmatrix}, \quad (26)$$

$$G_{pb} = \begin{bmatrix} 0 \\ \psi^2 \end{bmatrix}, \quad (27)$$

and

$$H_{pb} = \begin{bmatrix} 1 & 0 \\ 0 & 1 \end{bmatrix}. \quad (28)$$

From Equation (19), an SMO for each pitch subsystem can be written as

$$\dot{\hat{x}}_{pb}(t) = F_{pb}\hat{x}_{pb}(t) + G_{pb}u_{pb}(t) - K_l e_y(t) + K_{nl}w_{pb}(t) \quad (29)$$

$$\hat{y}_{pb}(t) = H_{pb}\hat{x}_{pb}(t) \quad (30)$$

where $\hat{x}_{pb}(t)$ and $\hat{y}_{pb}(t)$ denote the estimated states and outputs, respectively. K_l and K_{nl} are fixed appropriate gain matrices selected to ensure the stability and convergence of the error dynamics. $w_{pb}(t)$ represents a discontinuous switched output estimation error injected into the SMO to induce a sliding motion and is given by

$$w_{pb}(t) = \begin{cases} -\sigma \|M_2\| \frac{P_2 H_{pb} e_x(t)}{\|P_2 H_{pb} e_x(t)\|} & \text{if } H_{pb} e_x(t) \neq 0 \\ 0 & \text{otherwise} \end{cases} \quad (31)$$

To verify the convergence of the SMO, the simulation diagram shown in Figure 2 is used. The parameters used to simulate the pitch system model are listed in Table 1.

Table 1. Parameters of the wind turbine model.

Symbol	Description	Value
b_r	viscous friction of the low-speed shaft	7.11 Nms/rad
b_g	viscous friction of the high-speed shaft	45.6 Nms/rad
ζ	damping factor	0.6
ψ	natural frequency	11.11 rad/s
h_{dt}	torsion damping coefficient	775.49 Nms/rad
k_{dt}	torsion stiffness	2.7×10^9 Nm/rad
J_r	moment of inertia of the low-speed shaft	55×10^6 Kg.m ²
J_g	moment of inertia of the high-speed shaft	390 Kg.m ²
N_g	gear ratio	95
η_{dt}	efficiency of the drive train	0.97

For simulation purposes, the input to the pitch system is set as a step signal of magnitude 10 and it is considered fault-free, that is, $f_a(t) = 0$, and the fault coupling matrix is set as $M_{pb} = [0, 0]^T$. The SMO initial conditions are set as zero, while the initial conditions of the states of the pitch system are set as 5 and -10 , respectively. The linear and nonlinear gain matrices of the SMO are given as:

The linear and nonlinear gain matrices of the SMO are given as

$$K_l = \begin{bmatrix} 5 & 1 \\ -123.43 & -9.332 \end{bmatrix} \quad (32)$$

and

$$K_{nl} = \begin{bmatrix} 1 & 0 \\ 0 & 1 \end{bmatrix}. \quad (33)$$

The Lyapunov design matrix P_2 for the switched signal is defined as

$$P_2 = \begin{bmatrix} 0.1 & 0 \\ 0 & 0.125 \end{bmatrix} \quad (34)$$

the design matrix $M_2 = 1$, and the scalar $\sigma = 6$.

The results of the SMO convergence are shown in Figures 4 and 5. Figure 4 shows both the pitch angle estimation and the pitch angle estimation error. It can be seen that the observer estimate converges asymptotically to the system state even if their initial conditions are different; therefore, the convergence of the SMO is assured. It can be observed that after 0.5 s, a sliding motion takes place, i.e., the estimation error is forced to reach and subsequently remain on the sliding surface and, thus, a sliding mode motion is said to take place.

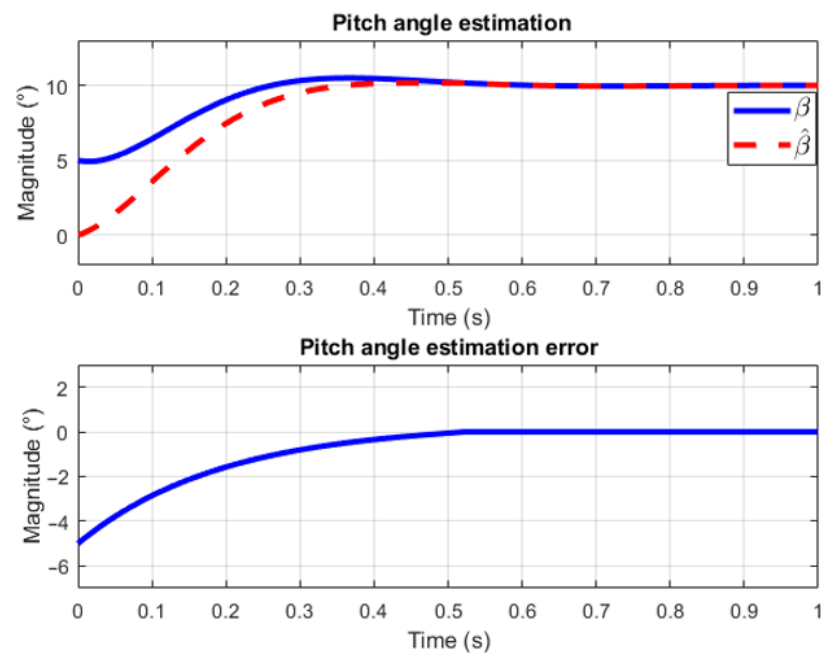


Figure 4. Convergence of the pitch angle estimation.

Figure 5 shows both the pitch speed estimation and the pitch speed estimation error. It can be seen that the estimated state converges asymptotically to the system state after approximately 0.6 s. This is indicative that a sliding motion is taking place on the sliding surface. It is important to mention that the difference in the speed of convergence in the estimation of each state variable is due to the fact that the initial conditions of the state variables are different.

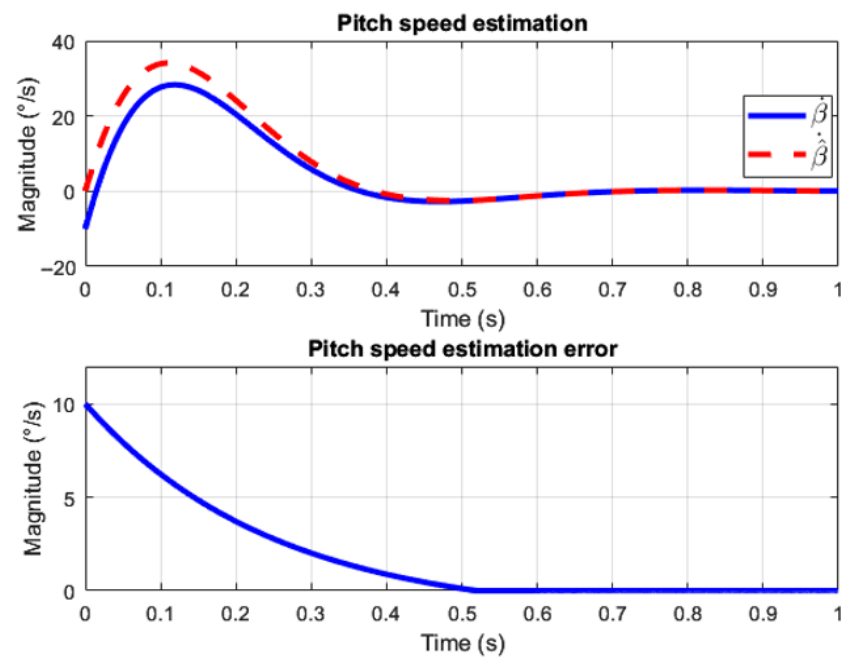


Figure 5. Convergence of the pitch speed estimation.

2.3.2. Actuator FDI Scheme for the Drive Train System

Actuator faults in the drive train system of a wind turbine can have significant consequences for the safety and operation of the wind turbine. Actuator faults in the drive train can be caused by various factors, including mechanical wear and tear, electrical faults, and environmental factors such as temperature and moisture. One common actuator fault in the drive train is caused by gear tooth damage, which inevitably results in gear ratio changes. The friction coefficient in the drive train changes slowly with time and can evolve over months or years. This change can also result in changes in the dynamics of the drive train system. The drive train system bearings are also likely to be faulty. Fatigue and wear due to heavy loads are inevitable. Moreover, pitting and impending cracks are also causes of faults. Generally, faults in the drive train system require time-consuming and costly maintenance. In order to reduce the potential impact of these faults in the drive train system, an effective fault diagnosis scheme is needed.

The drive train system connects the low-speed shaft to the high-speed shaft of the wind turbine. From the mathematical representation of the drive train shown in Equations (4)–(6), it can be observed that it has two input channels, namely, the rotor and the generator torque. Actuator faults are considered to occur in both the rotor and generator torques. However, since the case of simultaneous failures rarely occurs, we consider that only one actuator fault occurs at a time; that is, the case of simultaneous faults is not considered. Actuator fault signals are modeled as additive bounded signals acting in each input channel of the drive train system. It is important to note that the rotor torque cannot be measured; therefore, different approaches have been proposed to estimate it. Because the focus of this study is on the design of an actuator fault reconstruction scheme and not on the actuator itself, it is assumed that the rotor torque is known.

Figure 6 shows the proposed scheme for performing actuator fault detection and isolation in the drive train system. It considers the design of a single SMO to estimate both states and outputs. The difference between the measured drive train variables and the observer outputs is injected into the SMO using a nonlinear function. This term forces the output estimation error to zero in finite time and compensates for the effects of actuator faults in the SMO to maintain a sliding motion. Because the drive train system has two measured outputs, the nonlinear output error injection term is a two-dimensional vector. Each component of this vector is injected into only one input channel of the drive train

system in such a way that it compensates only the actuator fault acting on its corresponding input channel. By independently filtering each component of the nonlinear output error injection vector, both fault reconstruction and fault isolation in the drive train system are achieved.

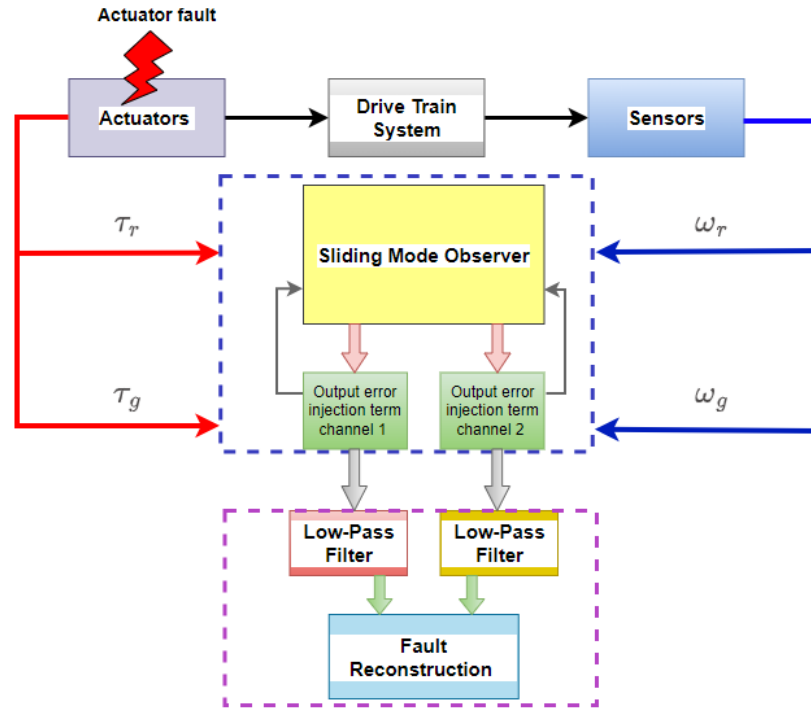


Figure 6. Actuator FDI scheme for the drive train system.

The SMO methodology presented in previous sections is applied below to the drive train system model. For the design of the SMO, it is considered that the drive train model in state space is written as

$$\dot{x}_{dt}(t) = F_{dt}x_{dt}(t) + G_{dt}u_{dt}(t) + M_{dt}f_a(t) \tag{35}$$

$$y_{dt}(t) = H_{dt}x_{dt}(t) \tag{36}$$

where $x_{dt}(t) \in \mathbb{R}^3$ is the state vector, $u \in \mathbb{R}^2$ is the input vector, $y_{dt}(t) \in \mathbb{R}^2$, $f_a(t)$ is any actuator fault signal, M_{dt} is a fault distribution matrix, and F_{dt} , G_{dt} , and H_{dt} are matrices defined as

$$F_{dt} = \begin{bmatrix} -\frac{h_{dt}+b_r}{J_r} & \frac{h_{dt}}{N_g J_r} & -\frac{k_{dt}}{J_r} \\ \frac{\eta_{dt}h_{dt}}{N_g J_g} & \frac{-\eta_{dt}h_{dt}-b_g}{N_g^2} & \frac{\eta_{dt}k_{dt}}{N_g J_g} \\ 1 & -\frac{1}{N_g} & 0 \end{bmatrix}, \tag{37}$$

$$G_{dt} = \begin{bmatrix} \frac{1}{J_r} & 0 \\ 0 & -\frac{1}{J_g} \\ 0 & 0 \end{bmatrix}, \tag{38}$$

and

$$H_{dt} = \begin{bmatrix} 1 & 0 & 0 \\ 0 & 1 & 0 \end{bmatrix} \tag{39}$$

From Equation (19), the sliding mode observer for the drive train system model can be written as

$$\dot{\hat{x}}_{dt}(t) = F_{dt}\hat{x}_{dt}(t) + G_{dt}u_{dt}(t) - K_l e_y(t) + K_{nl} w_{dt}(t) \tag{40}$$

$$\hat{y}_{dt}(t) = H_{dt}\hat{x}_{dt}(t) \quad (41)$$

where $\hat{x}_{pb}(t)$ and $\hat{y}_{pb}(t)$ denote the estimate of state and output, respectively. K_l and K_{nl} are appropriate gain matrices selected to ensure the stability and convergence of the dynamics of error, and $w_{dt}(t)$ represents a discontinuous switched component to induce a sliding motion in the SMO. To verify the convergence of the SMO, the simulation diagram shown in Figure 2 was implemented. The parameters used to simulate the drive train system model are shown in Table 1. The linear and nonlinear gain matrices of the observer are given as

$$K_l = \begin{bmatrix} 10 & -0.0035 \\ 0.0203 & 19.8829 \\ 1 & -0.0095 \end{bmatrix} \quad (42)$$

$$K_{nl} = \begin{bmatrix} 1 & 0 \\ 0 & 1 \\ 0 & 0.0001 \end{bmatrix}, \quad (43)$$

and the nonlinear output error injection signal $w_{dt}(t)$ is given as

$$w_{dt}(t) = \begin{cases} -\sigma \|M_2\| \frac{P_2 H_{dt} e_x(t)}{\|P_2 H_{dt} e_x(t)\|} & \text{if } H_{dt} e_x(t) \neq 0 \\ 0 & \text{otherwise} \end{cases} \quad (44)$$

where the scalar $\sigma = 6$, the design matrix $P_2 = [0.1, 0; 0, 0.125]$, the matrix $M_2 = 1$, and the estate estimation error is defined as $e_x(t) = \hat{x}_{dt}(t) - x_{dt}(t)$. For simulation purposes, the two inputs of the drive train system are set as step-type signals of magnitude 10 and 100, respectively. For the time being, the system is considered fault-free, that is, $f_a(t) = 0$, and the fault coupling matrix $M_{dt} = [0, 0, 0]^T$. The observer initial conditions are considered to be zero, while the initial conditions for the drive train system are chosen as $x_{dt} = [1, -1, 1]^T$. The results of both observer outputs and output estimation errors are shown in Figures 7 and 8. Figure 7 shows that after approximately 1.2 s, a perfect tracking between system output and observer output is achieved and, therefore, a sliding motion takes place, i.e., the output estimation error is forced to reach and subsequently remain on the sliding surface. It can be seen that once the sliding motion is achieved, the state estimation errors evolve according to a first-order decay.

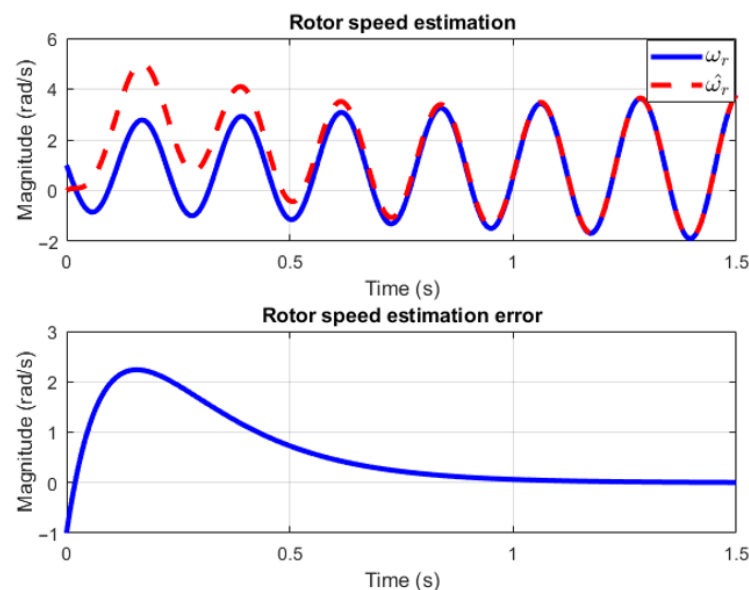


Figure 7. Convergence of the rotor speed estimation.

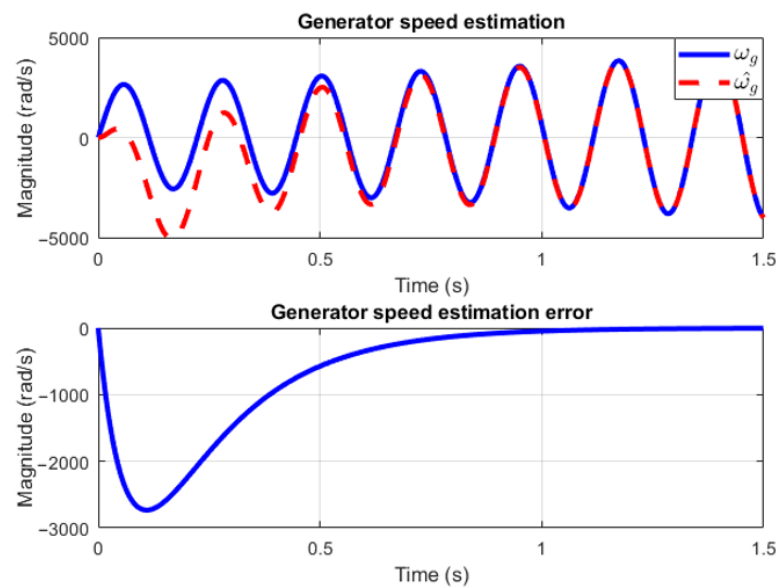


Figure 8. Convergence of the generator speed estimation.

3. Results

In this section, the results of the proposed SMO-based FDI scheme are presented. To evaluate the effectiveness of the proposed FDI scheme, a set of different actuator faults on a wind turbine benchmark model are employed. The test only considers actuator faults in the pitch and the drive train systems. Bounded actuator faults modeled as additive signals are considered. The actuator faults are applied to the input channels of both the pitch and the drive systems. The faults are set as follows:

- Fault 1: A sinusoidal fault signal presented in pitch system 1 given by $f_{a1} = 5 \times \sin(0.5t)$ in the time period from 2.5133 to 47.7522 s.
- Fault 2: A sinusoidal fault signal presented in pitch system 2 given by $f_{a2}(t) = 5 \times \sin(0.5t)$ in the time period from 0 to 50 s.
- Fault 3: A sinusoidal fault signal presented in pitch system 3 given by $f_{a3}(t) = 10 \times \sin(0.5t)$ in the time period from 0 to 50 s.
- Fault 4: A square fault signal presented in the rotor torque of the drive train system given by $f_{a4}(t) = 5 \times \text{square}(0.5t)$ in the time period from 6.2832 to 40.2100 s.
- Fault 5: A sinusoidal fault signal presented in the generator torque of the drive train system given by $f_{a5}(t) = 5 \times \sin(0.5t)$ in the time period from 1.2566 to 37.6991 s.
- Fault 6: A sawtooth fault signal presented in the generator torque of the drive system given by $f_{a6}(t) = 5 \times \text{sawtooth}(0.5t)$ in the time period from 10.0531 to 43.9800 s.

3.1. Results of the FDI Scheme in the Pitch System

The problem of fault detection and isolation in the pitch system is solved by using the architecture shown in Figure 3. Since the output error injection signal injected into the SMO compensates for the dynamics added by the faults in the pitch system, the sliding motion is not interrupted, even in the presence of actuator faults. The dynamic of these faults is recovered using an LPF implemented through a first-order differential equation. By choosing the time constant of the filter to be tiny, but larger than the sampling time used on the computer to implement the LPF, the dynamics of the faults in the pitch system can be reconstructed accurately.

To measure how much better the method is at reproducing the actuator fault in the system, the normalized root mean square error (NRMSE) criterion is used, which proportions a fit percentage value.

The simulation of the proposed FDI scheme in the pitch system is obtained considering the initial conditions of the SMO to be zero, while the initial conditions of the pitch

system states are set as $x_{pb}(t) = [2 - 1]^T$. The system input has been arbitrarily set as a step function of magnitude 10. The fault lock matrix for the pitch actuator is chosen as $M_{pb} = [0, 1]^T$ and the scaling parameter of the nonlinear output error injection term is chosen as $\sigma = 6$.

The results of the reconstruction of Fault 1 in pitch system 1 are shown in Figure 9. In order to obtain the highest accuracy in the actuator fault reconstruction, a heuristic process is performed to find the best choice of the LPF time constant. In Table 2, three different filter time constants are presented. From the results obtained, it can be concluded that the best fit is achieved by using a time constant of 0.06 s, with which a fit percentage of 82.9103% is obtained.

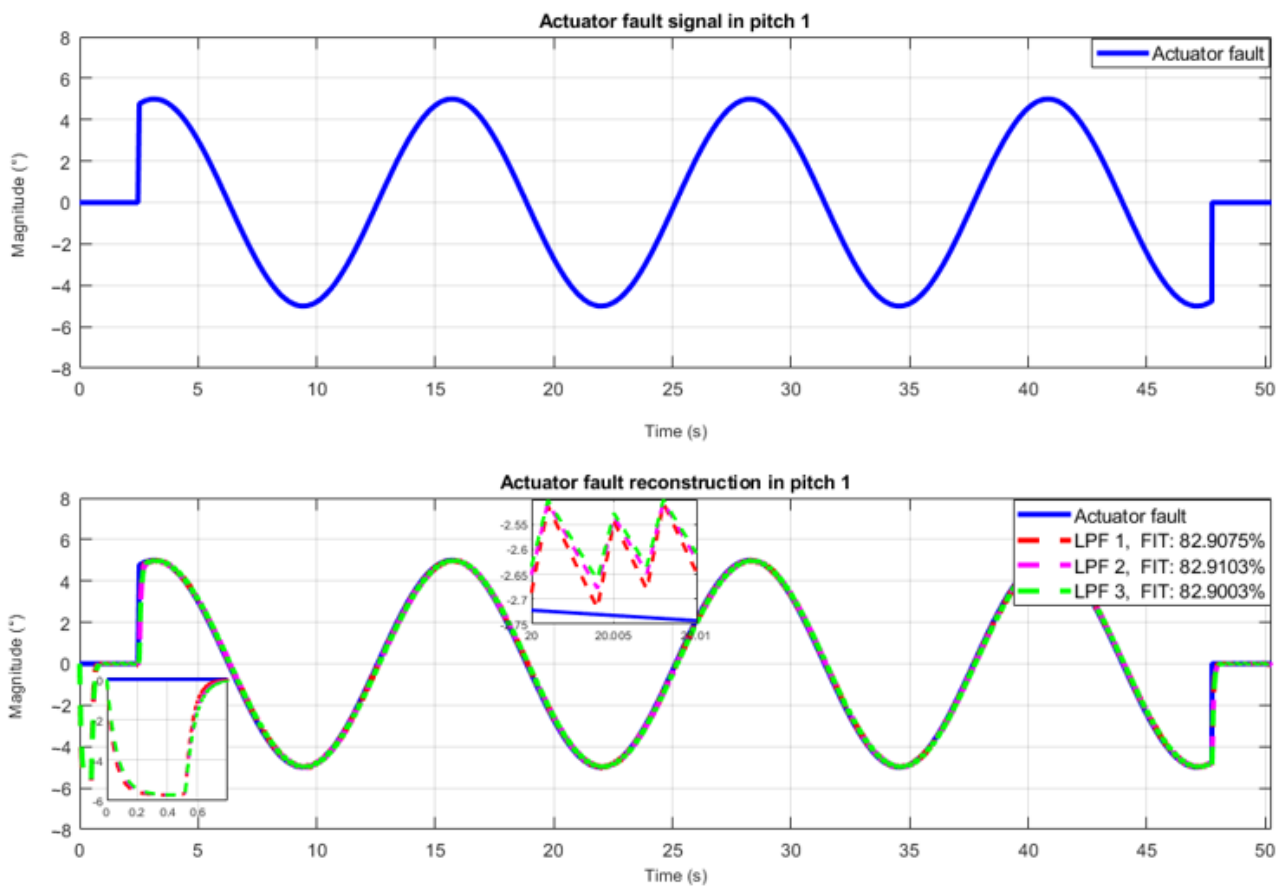


Figure 9. Reconstruction of actuator Fault 1 in pitch system 1.

Table 2. Results of the actuator fault reconstruction in the pitch system.

Faults	Time Constant LPF 1 [s]	Time Constant LPF 2 [s]	Time Constant LPF 3 [s]	Best FIT [%]
Fault1	0.050	0.06	0.065	82.9103
Fault2	0.085	0.09	0.095	82.8394
Fault3	0.020	0.03	0.040	67.1775

Figure 10 shows the results of the actuator fault reconstruction in pitch system 2. It can be seen that the best-fit percentage is obtained with LPF 2, which is implemented with a time constant of 0.09 s (see Table 2).

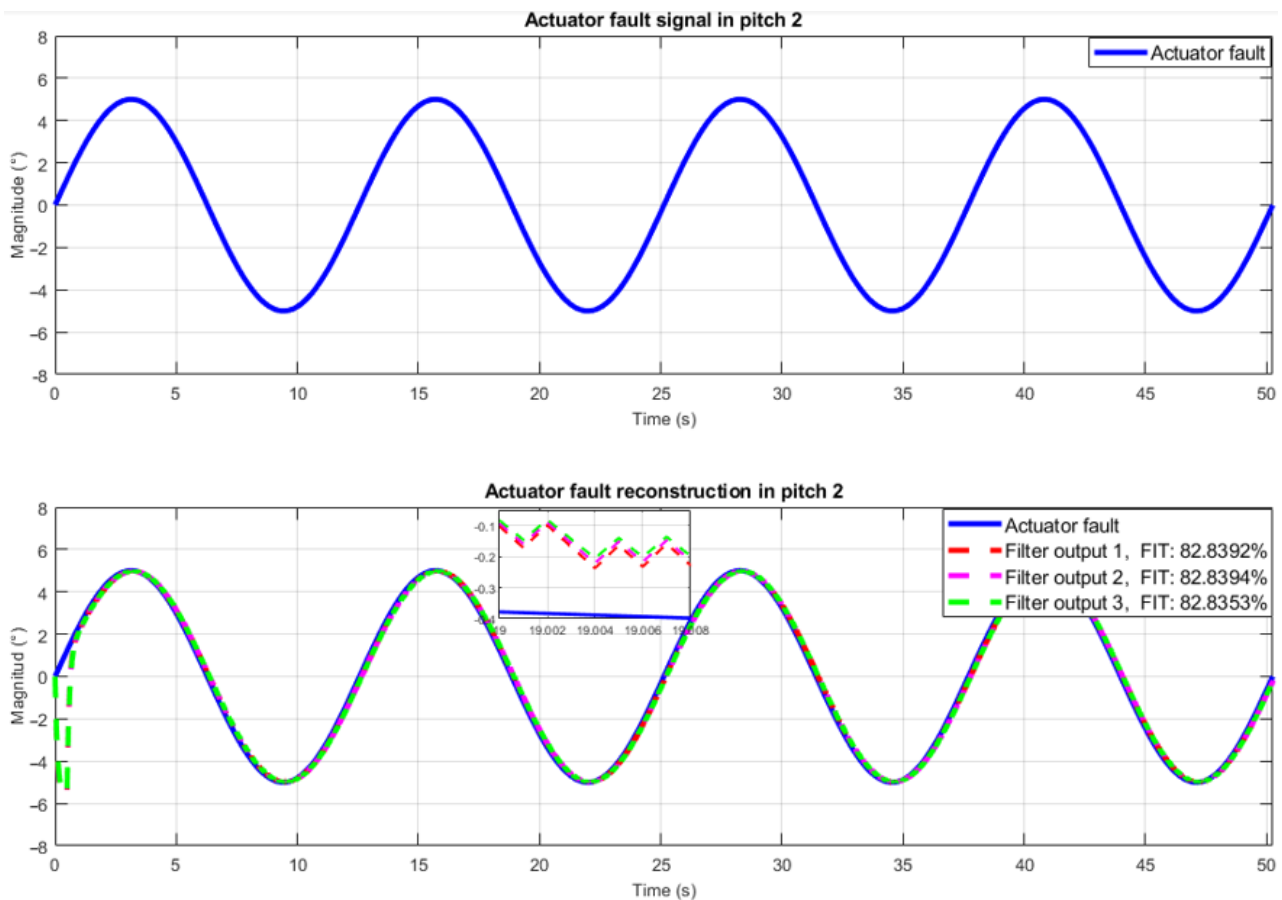


Figure 10. Reconstruction of actuator Fault 2 in the pitch system 2.

It is important to underline that for a sliding motion to take place and, subsequently, for it to be maintained in the presence of actuator faults, it is necessary to select the scalar σ so that the inequality $\sigma > \|f_a(t)\|$ is satisfied for all $t_0 > 0$. Since Faults 1 and 2 satisfy this condition, the sliding motion is maintained despite the dynamics introduced by the actuator faults. This ensures that an accurate reconstruction of the faults can be performed, as shown in Figures 9 and 10.

In the time intervals where inequality $\sigma > \|f_a(t)\|$ is not fulfilled, two issues occur; the first is that the sliding motion cannot be maintained and the second is that the matched disturbance rejection property is lost and, therefore, it is not possible to perform the actuator fault reconstruction.

Figure 11 shows the results of the actuator FDI scheme for Fault 3. It can be observed that since the boundary of Fault 3 is greater than the scalar σ , the inequality $\sigma > \|f_{a3}(t)\|$ cannot be verified for all $t_0 > 0$. This impedes the achievement of an adequate reconstruction of Fault 3 in the intervals where the amplitude fault is greater than the scalar σ , as shown in Figure 11.

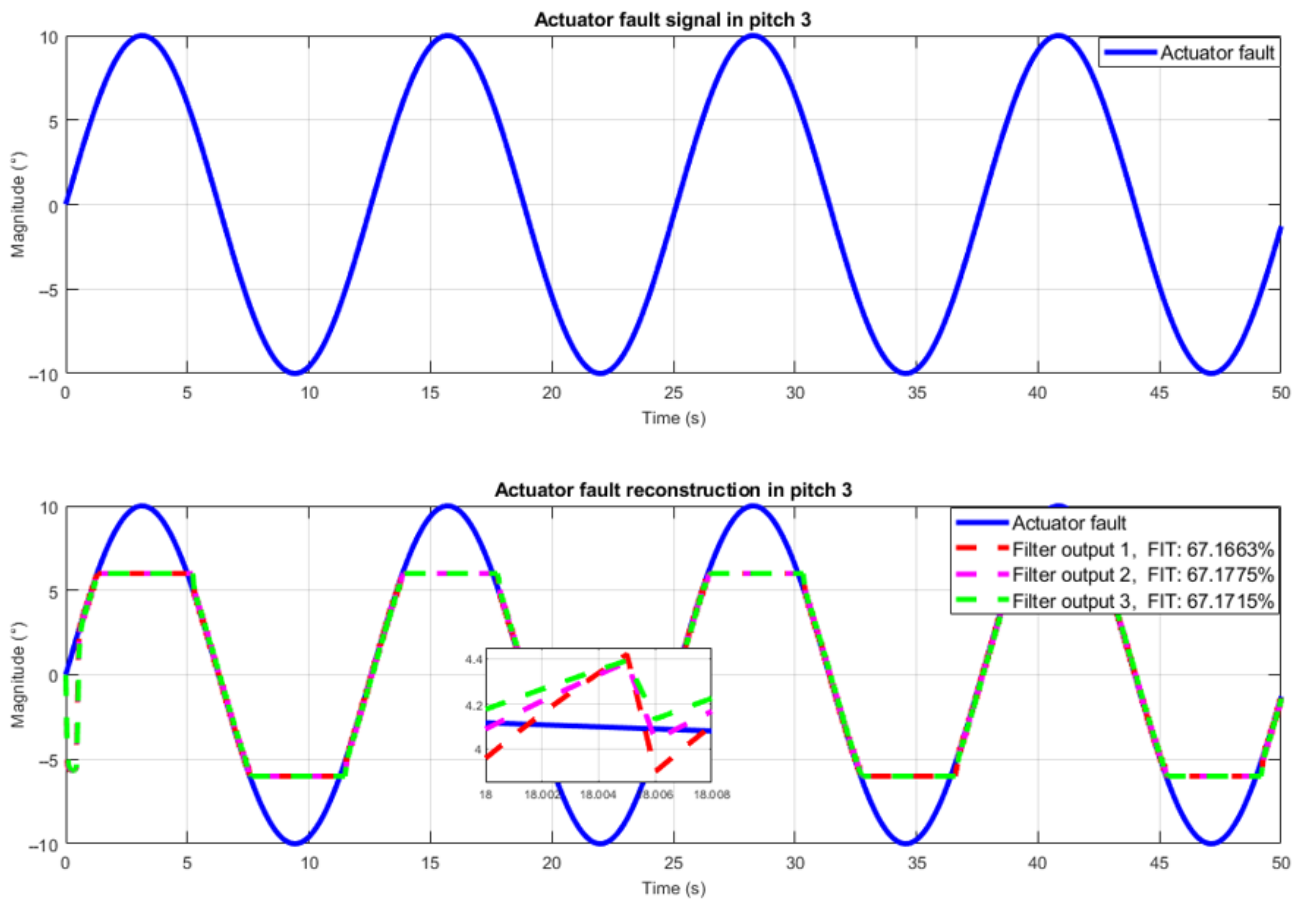


Figure 11. Reconstruction of actuator Fault 3 in the pitch system 3.

3.2. Results of the FDI Scheme in the Drive Train System

To solve the fault isolation problem in the drive train system, the proposed scheme shown in Figure 6 is implemented. Two different LPFs are used to isolate the actuator faults, acting on each one of the input channels of the drive train system. When an actuator fault occurs in channel 1 of the system, the output of LPF 1 is expected to reconstruct the fault while the output of LPF 2 remains at zero because the second input channel of the system is free of fault.

The fault detection problem is solved using the estimation approach described earlier (see Section 2). The main objective of the proposed approach is to maintain the sliding motion even in the presence of actuator faults. The second objective is to recover the fault dynamic through a filtering process of the output error injection signal, which is used to keep the dynamic in a sliding motion. The filtering process is performed using an LPF, which is implemented by a first-order differential equation. To evaluate the effectiveness of the reconstruction, NRMSE analysis, which proportioned a fit percentage number, is used.

The simulation of the proposed FDI scheme for the drive train system has been obtained considering the initial conditions of the SMO to be $\hat{x}(t) = [0, 0, 0]^T$, while the initial conditions of the drive train system are established as $x_{dt}(t) = [1, -1, 1]^T$.

The fault lock matrix for rotor torque fault is set as $M_{dt} = [1, 0, 0]^T$, while that for generator torque fault is set as $M_{dt} = [0, 1, 0]^T$. The scalar σ is chosen as 6. System inputs and the SMO gains are selected as stated in Section 2.

Figure 12 shows Fault 4 acting on the first input channel of the system, which affects the signal of the rotor torque. Since the sliding motion is maintained despite the presence of a fault, by passing the nonlinear output error injection term of channel 1 through LPF 1, the

fault reconstruction is achieved. From a heuristic process, the optimal filter time constant is 0.0150 s, with a fit of 90.6006%.

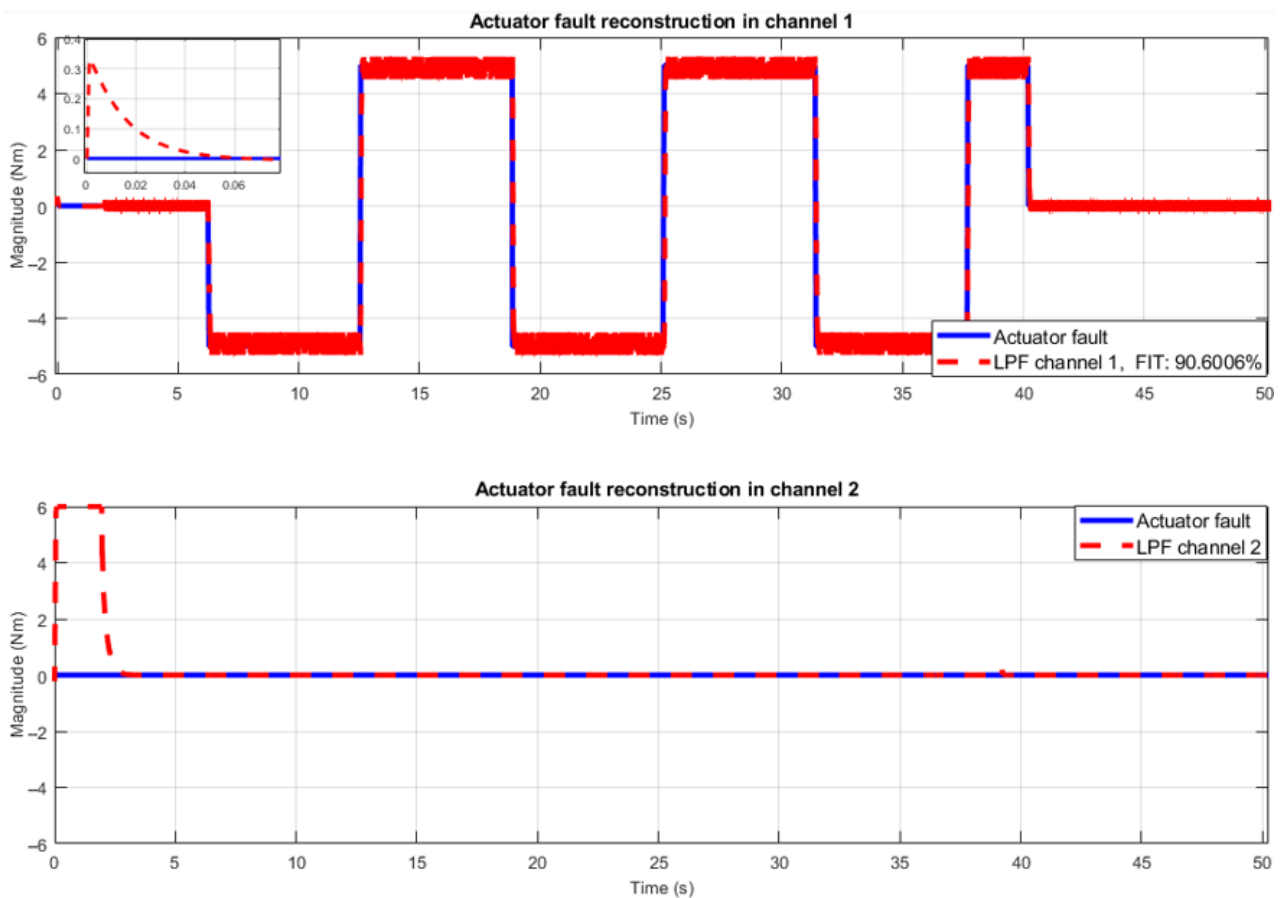


Figure 12. Reconstruction of actuator Fault 4 in the drive train system.

As LPF 2 filters the output error injection term injected into channel 2 of the SMO and it is free of fault, it can be seen that its output remains at zero. It is important to note that the zero deviation in the output of LPF 2 at the start of the simulation is due to the delay introduced by the filter. This delay is also present in the reconstruction of the fault. It can be observed that after the delay introduced by the filtering process, fault isolation and reconstruction are carried out precisely.

Figure 13 shows the fault reconstruction when Fault 5 is acting in the second input channel of the drive train. Since the inequality $\sigma > \|f_{a5}(t)\|$ is satisfied for all $t_0 > 0$, by applying an LPF with a time constant of 0.04 s, a fit of 90.1299% is achieved in the fault reconstruction. It can be observed that during the time the fault remains active, the output of LPF of channel 1 remains at zero, which indicates that the fault is present in channel 2 of the system. Hence, it can be established that the fault is properly isolated.

Figure 14 shows the results of the reconstruction of sawtooth Fault 6. Since Fault 6 is applied in the second input channel of the drive train system, by filtering the output error injection term injected into channel 2 with an LPF whose time constant is 0.024 s, a fit of 87.2779% is obtained.

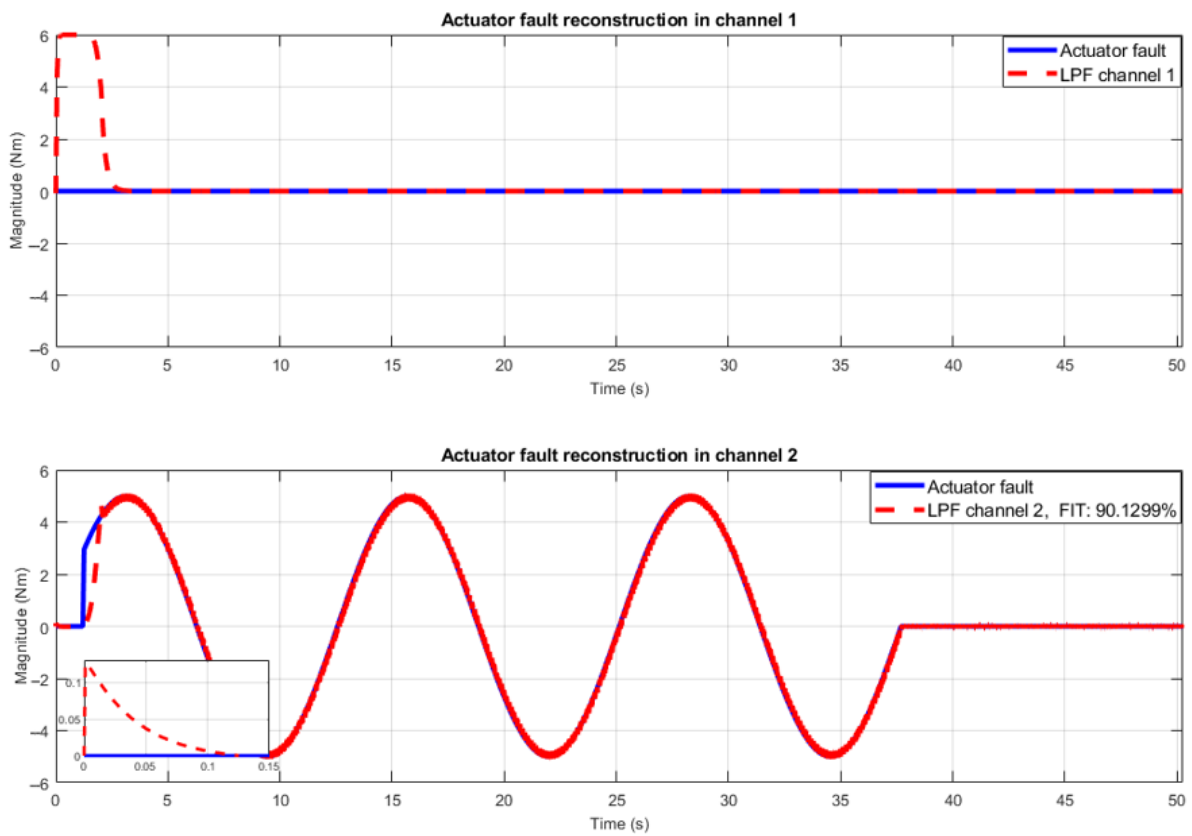


Figure 13. Reconstruction of actuator Fault 5 in the drive train system.

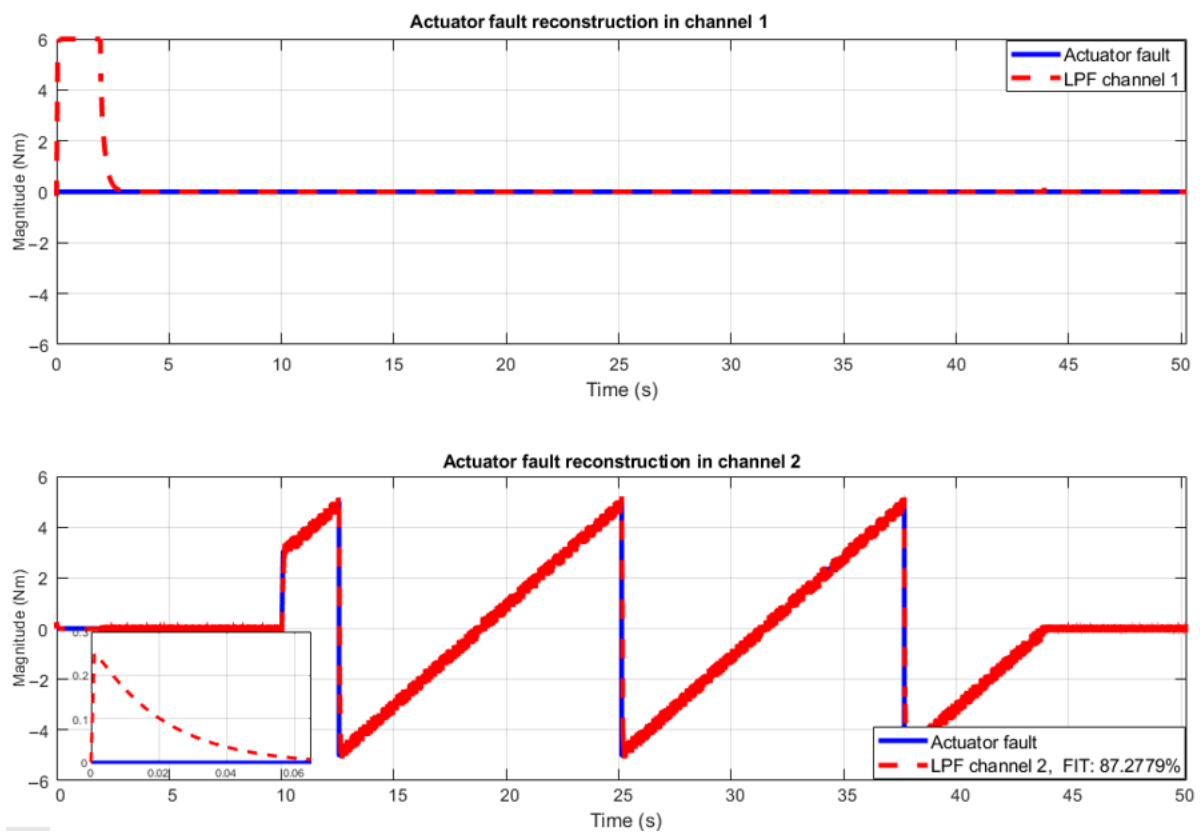


Figure 14. Reconstruction of actuator Fault 6 in the drive train system.

From the output of the LPF applied to the output error injection term injected into channel 1, it can be seen that it remains at zero during the time that the fault is active. Therefore, it can be concluded that the fault occurred in channel 2 of the system. Table 3 presents the time constants used in the LPF for each of the faults in the drive train system, as well as the best fit in percentage obtained when performing the fault reconstruction.

Table 3. Results of the actuator fault reconstruction in the drive train system.

Faults	Time Constant LPF [s]	Best FIT [%]
Fault 4	0.0150	90.6006
Fault 5	0.0400	90.1299
Fault 6	0.0200	87.2779

3.3. Factors Affecting the Fault Reconstruction Performance

Several factors can affect the performance of fault reconstruction using an SMO in wind turbines. Here are some key factors to consider:

1. The characteristics of the faults themselves can impact the performance of fault reconstruction. From the results presented in Section 3, it is noted that factors such as fault magnitude, fault duration, and fault dynamics (e.g., abrupt or gradual changes) affect the accuracy of the fault reconstruction. Different types of faults require specific adaptations in both the SMO design (the σ -parameter) and the LPF time constant to ensure effective fault estimation.
2. The design of the SMO, including its parameter selection and initial conditions, affects the fault reconstruction performance. In order to implement the SMO-based FDI scheme in a wind turbine, the initial condition of the observer must be assigned prior to the beginning of the wind turbine operation. However, the issue of how best to choose those initial condition values has apparently been completely ignored in control engineering textbooks. As a consequence, observer initial conditions in industrial applications are usually set to zero by default. A study of the effect of the SMO initial conditions on the performance of the fault reconstruction was realized. Table 4 shows Fault 5 reconstruction performance using different SMO initial conditions, keeping the initial condition of the drive train system fixed. From the results, it can be noted that for SMO initial conditions close to system conditions, reconstruction performance improves, while for SMO initial conditions far from the initial conditions of the system, the performance worsens. This is an expected result since the choice of initial conditions impacts the transient behavior and convergence speed of the SMO.

Table 4. Effects of the SMO initial conditions in Fault 5 reconstruction.

Initial Conditions	Time Constant LPF [s]	Best FIT [%]
$\hat{x} = [0 \ 0 \ 0]^T$	0.0400	90.1299
$\hat{x} = [0 \ 0 \ 1]^T$	0.0400	92.2562
$\hat{x} = [3 \ 2 \ 3]^T$	0.0350	88.5118
$\hat{x} = [5 \ 5 \ 4]^T$	0.0350	87.5168
$\hat{x} = [100 \ 90 \ 100]^T$	0.0350	79.2138

The observer's parameters should be appropriately chosen to achieve fast and accurate estimation of both system states and fault signals. Improper observer design can result in slow convergence, estimation errors, or undesirable oscillations in the reconstructed fault signals. A study of the effect of the SMO σ -parameter on the performance of the fault reconstruction was realized. Table 5 shows Fault 5 reconstruction performance using different values of the σ -parameter. From the results, it is noted that for σ values less than the magnitude of the fault, a substantial degradation in the reconstruction of Fault 5 is

observed. However, increasing the σ value does not substantially improve the performance of the fault reconstruction. Consequently, an appropriate selection of the σ value must satisfy the condition $\sigma > \|f_a(t)\|$.

Table 5. Effects of σ in Fault 5 reconstruction.

Parameter σ	Time Constant LPF [s]	Best FIT [%]
$\sigma = 6$	0.0400	90.1299
$\sigma = 5$	0.0350	89.8022
$\sigma = 3$	0.0350	66.5234
$\sigma = 8$	0.0400	90.5583
$\sigma = 10$	0.0450	90.7927
$\sigma = 20$	0.0800	90.9546

- From the point of view of the implementation of the proposed scheme, factors such as sampling rate and computational resources can affect the fault reconstruction performance. The sampling rate at which sensor data are collected and processed affects the temporal resolution of fault reconstruction. A higher sampling rate allows for finer detection and tracking of fault dynamics, but it also increases computational requirements. The sampling rate should be chosen carefully to balance the need for accuracy with practical implementation considerations. Moreover, the computational resources available for implementing the SMO influence its performance. A higher computational capability enables faster calculations and can facilitate real-time fault reconstruction. Insufficient computational resources may result in slower estimation or limitations in the complexity of the observer algorithm.
- The selection and quality of sensors used to measure the system outputs and inputs also impact the performance of fault reconstruction. High-quality sensors with low noise and suitable measurement range contribute to accurate state estimation.

4. Discussion

An observer-based FDI scheme that uses a particular class of SMO to identify and isolate actuator faults using an estimation approach was presented. Fault detection and fault isolation problems are solved by analyzing the nonlinear output error injection signal required to keep the SMO in a sliding motion. The proposed actuator FDI scheme is evaluated with six different actuator faults, and the accuracy of the proposed approach is validated using the NRMSE method. In contrast to the works presented in [20,23] a simple architecture using an LPF is shown to be sufficient to perform an accurate fault reconstruction, with no false alarm or missed detection.

The proposed FDI scheme does not require explicit information from the fault. The only fault information required is the fault to be bounded. Thus, the actuator fault reconstruction signal is obtained online and without prior knowledge of the fault, which is of vital importance for the FDI scheme to be implemented in real applications.

It is important to highlight, however, that the dynamics of faults, the filter time constant, the observer initial conditions, and the σ value of the SMO affect fault reconstruction accuracy. To find the optimal filter time constant, a heuristic process is used. However, a method to automatically find the optimal filter time constant could be used. The initial conditions of the SMO were shown to affect the fault reconstruction performance. A better fault reconstruction performance is achieved with SMO initial conditions close to the initial condition of the system.

The σ value was shown to have an impact on the fault reconstruction accuracy. If the σ value is smaller than the upper bound of the fault, an accurate fault reconstruction is not possible. However, values of σ much larger than the upper bound of the fault were not shown to lead to a significant increase in the fault reconstruction precision. Furthermore, high values of σ were shown to have a prejudicial effect on the accuracy of state estimation due to the undesirable phenomenon known as chattering.

5. Conclusions

In this paper, an actuator observer-based FDI scheme for the pitch and drive train systems of a wind turbine is proposed. The proposed scheme employs a special class of SMOs that have the capacity to drive the output estimation error to zero in finite time, even in the presence of actuator faults. The approach adopted here uses the nonlinear output estimation error signal to perform actuator fault reconstruction. This error signal is used to drive the observer dynamics and converges the estimated output to the actual output of the system. Thus, it compensates for fault dynamics in the SMO by switching at high frequency as a function of the output estimation error. To reconstruct actuator faults in both the pitch and drive systems, an approach using an LPF on the nonlinear output estimation error signal is adopted. The actuator fault reconstruction signal is obtained online and without prior knowledge of the fault and, thus, it is easy to implement in real time. Factors such as the initial conditions and SMO settings were demonstrated to influence the fault reconstruction performance. The simulation results and NRMSE analysis have demonstrated the effectiveness of the proposed scheme for performing actuator fault reconstruction. In future work, the SMO-based FDI scheme will be integrated with an FTC system.

Author Contributions: Conceptualization, V.B.-J. and M.A.-M.; methodology, V.B.-J. and M.A.-M.; software, V.B.-J. and J.G.-M.; validation, V.B.-J. and M.A.-M.; formal analysis, G.V.G.-R. and V.B.-J.; investigation, V.B.-J., M.A.-M. and B.Y.L.-Z.; resources, G.V.G.-R., B.Y.L.-Z., E.M.S.-C. and J.G.-M.; writing—original draft preparation, V.B.-J., B.Y.L.-Z., J.G.-M. and E.M.S.-C.; writing—review and editing, M.A.-M., E.M.S.-C., V.B.-J., B.Y.L.-Z., G.V.G.-R. and J.G.-M.; supervision, V.B.-J. All authors have read and agreed to the published version of the manuscript.

Funding: This research received no external funding.

Data Availability Statement: Not applicable.

Acknowledgments: The development of this project is the product of the support provided by the National Council of Science and Technology (CONACYT) and the National Center for Technological Research and Development (CENIDET).

Conflicts of Interest: The authors declare no conflict of interest.

Abbreviations

The following abbreviations are used in this manuscript:

SMO	Sliding mode observer
FDI	Fault detection and isolation
NEMSE	Normalized root mean square error
DNN	Deep neural networks
PCA	Principal component analysis
LPF	Low-pass filter
NREL	National Renewable Energy Laboratory
FTC	Fault-tolerant control

Nomenclature

Matrix

F	System matrix
G	Input matrix
H	Output matrix
K	Observer gain matrix
M	Fault distribution matrix
P	Symmetric positive definite matrix
T	Change of coordinates matrix

Vectors

u	System input vector
e	Estimation error vector
x	System state vector

\hat{x}	Estimate of states vector
y	System output vector
\hat{y}	Estimate of output vector
w	Nonlinear discontinuous function
Constants	
b	Viscous friction constant
h	Torsion damping constant
j	Moment of inertia constant
k	Torsion stiffness constant
N	Gear ratio constant
r	Rotor ratio constant
n	Real number
p	Real number
m	Real number
q	Real number
Signals	
f	Fault signal
v	Wind speed signal
E	Power electrical signal
Greek letters	
α	Scalar
β	Pitch angle
ξ	Damping coefficient
η	Efficiency
θ	Torsion angle
σ	Scalar
ψ	Natural frequency
γ	Cutoff frequency
λ	Tip speed ratio
ρ	Wind density
Subscripts	
a	Actuator
dt	Drive train
g	Generator
l	Linear
nl	Nonlinear
pb	Pitch blade
r	Rotor
ω	Wind
x	State
y	Output
ref	Reference

References

1. Global Wind Energy Council. *Global Wind Report 2022*; Global Wind Energy Council: Bonn, Germany, 2022.
2. Anaya-Lara, O.; Jenkins, N.; Ekanayake, J.B.; Cartwright, P.; Hughes, M. *Wind Energy Generation: Modelling and Control*; John Wiley & Sons: Chichester, UK, 2009.
3. Wymore, M.L.; Van Dam, J.E.; Ceylan, H.; Qiao, D. A survey of health monitoring systems for wind turbines. *Renew. Sustain. Energy Rev.* **2015**, *52*, 976–990. [[CrossRef](#)]
4. Luo, N.; Vidal, Y.; Acho, L. *Wind Turbine Control and Monitoring*; Springer: Cham, Switzerland, 2014; Available online: <http://www.springer.com/series/1412> (accessed on 4 January 2023).
5. Chang, C.C.W.; Ding, T.J.; Ariannejad, M.; Chao, K.C.; Samdin, S.B. Fault detection and anti-icing technologies in wind energy conversion systems: A review. *Energy Rep.* **2022**, *8*, 28–33. [[CrossRef](#)]
6. Thirumarimurugan, M.; Bagyalakshmi, N.; Paarkavi, P. Comparison of fault detection and isolation methods: A review. In Proceedings of the 2016 10th International Conference on Intelligent Systems and Control (ISCO), Coimbatore, India, 7–8 January 2016; pp. 1–6. [[CrossRef](#)]
7. Liu, Z.; Zhang, L. A review of failure modes, condition monitoring and fault diagnosis methods for large-scale wind turbine bearings. *Measurement* **2020**, *149*, 107002. [[CrossRef](#)]

8. Fekih, A.; Habibi, H.; Simani, S. Fault Diagnosis and Fault Tolerant Control of Wind Turbines: An Overview. *Energies* **2022**, *15*, 7186. [[CrossRef](#)]
9. Gao, Z.; Liu, X. An Overview on Fault Diagnosis, Prognosis and Resilient Control for Wind Turbine Systems. *Processes* **2021**, *9*, 300. [[CrossRef](#)]
10. Simani, S.; Castaldi, P. Intelligent Fault Diagnosis Techniques Applied to an Offshore Wind Turbine System. *Appl. Sci.* **2019**, *9*, 783. [[CrossRef](#)]
11. Liu, W. Intelligent fault diagnosis of wind turbines using multi-dimensional kernel domain spectrum technique. *Measurement* **2018**, *133*, 303–309. [[CrossRef](#)]
12. Wen, X.; Xu, Z. Wind turbine fault diagnosis based on ReliefF-PCA and DNN. *Expert Syst. Appl.* **2021**, *178*, 115016. [[CrossRef](#)]
13. Pashazadeh, V.; Salmasi, F.R.; Araabi, B.N. Data driven sensor and actuator fault detection and isolation in wind turbine using classifier fusion. *Renew. Energy* **2018**, *116*, 99–106. [[CrossRef](#)]
14. Liu, W.; Tang, B.; Han, J.; Lu, X.; Hu, N.; He, Z. The structure healthy condition monitoring and fault diagnosis methods in wind turbines: A review. *Renew. Sustain. Energy Rev.* **2015**, *44*, 466–472. [[CrossRef](#)]
15. Lan, J.; Patton, R.J. *Robust Integration of Model-Based Fault Estimation and Fault-Tolerant Control*; Springer: Berlin/Heidelberg, Germany, 2021. [[CrossRef](#)]
16. Yang, Y.; Ding, S.X.; Li, L. On observer-based fault detection for nonlinear systems. *Syst. Control Lett.* **2015**, *82*, 18–25. [[CrossRef](#)]
17. Teng, J.; Li, C.; Feng, Y.; Yang, T.; Zhou, R.; Sheng, Q.Z. Adaptive Observer Based Fault Tolerant Control for Sensor and Actuator Faults in Wind Turbines. *Sensors* **2021**, *21*, 8170. [[CrossRef](#)] [[PubMed](#)]
18. Odgaard, P.F.; Stoustrup, J.; Kinnaert, M. Fault-Tolerant Control of Wind Turbines: A Benchmark Model. *IEEE Trans. Control Syst. Technol.* **2013**, *21*, 1168–1182. [[CrossRef](#)]
19. Pujol-Vazquez, G.; Acho, L.; Gibergans-Báguena, J. Fault Detection Algorithm for Wind Turbines' Pitch Actuator Systems. *Energies* **2020**, *13*, 2861. [[CrossRef](#)]
20. Zhu, J.; Ma, K.; Hajizadeh, A.; Soltani, M.; Chen, Z. Fault detection and isolation for wind turbine electric pitch system. In Proceedings of the 2017 IEEE 12th International Conference on Power Electronics and Drive Systems (PEDS), Honolulu, HI, USA, 12–15 December 2017; pp. 618–623. [[CrossRef](#)]
21. Odgaard, P.F.; Stoustrup, J. Unknown input observer based detection of sensor faults in a wind turbine. In Proceedings of the 2010 IEEE International Conference on Control Applications, Yokohama, Japan, 8–10 September 2010; pp. 310–315. [[CrossRef](#)]
22. Hwang, I.; Kim, S.; Kim, Y.; Seah, C.E. A Survey of Fault Detection, Isolation, and Reconfiguration Methods. *IEEE Trans. Control Syst. Technol.* **2009**, *18*, 636–653. [[CrossRef](#)]
23. Chen, J.; Patton, R.J. Robust Model-Based Fault Diagnosis for Dynamic Systems. In *The International Series on Asian Studies in Computer and Information Science*; Springer: Boston, MA, USA, 1999; Volume 3. [[CrossRef](#)]
24. Ziyabari, S.H.S.; Shoorehdeli, M.A.; Karimirad, M. Robust fault estimation of a blade pitch and drivetrain system in wind turbine model. *J. Vib. Control* **2020**, *27*, 277–294. [[CrossRef](#)]
25. Edwards, C.; Spurgeon, S.K.; Patton, R.J. Sliding mode observers for fault detection and isolation. *Automatica* **2000**, *36*, 541–553. [[CrossRef](#)]
26. Alwi, H.; Edwards, C.; Tan, C.P. Fault Detection and Fault-Tolerant Control Using Sliding Modes. In *Advances in Industrial Control*; Springer: London, UK, 2011. [[CrossRef](#)]
27. Habibi, H.; Howard, I.; Simani, S.; Fekih, A. Decoupling Adaptive Sliding Mode Observer Design for Wind Turbines Subject to Simultaneous Faults in Sensors and Actuators. *IEEE/CAA J. Autom. Sin.* **2021**, *8*, 837–847. [[CrossRef](#)]
28. Borja-Jaimes, V.; Adam-Medina, M.; López-Zapata, B.Y.; Valdés, L.G.V.; Pachecano, L.C.; Coronado, E.M.S. Sliding Mode Observer-Based Fault Detection and Isolation Approach for a Wind Turbine Benchmark. *Processes* **2021**, *10*, 54. [[CrossRef](#)]
29. Chen, W.; Ding, S.; Haghani, A.; Naik, A.; Khan, A.; Yin, S. Observer-based FDI Schemes for Wind Turbine Benchmark. *IFAC Proc. Vol.* **2011**, *44*, 7073–7078. [[CrossRef](#)]
30. Habibi, H.; Howard, I.; Simani, S. Reliability improvement of wind turbine power generation using model-based fault detection and fault tolerant control: A review. *Renew. Energy* **2018**, *135*, 877–896. [[CrossRef](#)]
31. Witczak, M.; Rotondo, D.; Puig, V.; Nejjari, F.; Pazera, M. Fault estimation of wind turbines using combined adaptive and parameter estimation schemes. *Int. J. Adapt. Control Signal Process.* **2017**, *32*, 549–567. [[CrossRef](#)]
32. Sun, X.; Patton, R.J. Robust actuator multiplicative fault estimation with unknown input decoupling for a wind turbine system. In Proceedings of the Conference on Control and Fault-Tolerant Systems (SysTol), Nice, France, 9–11 October 2013; pp. 263–268. [[CrossRef](#)]
33. Isermann, R. *Fault-Diagnosis Systems: An Introduction from Fault Detection to Fault Tolerance*; Springer: Berlin/Heidelberg, Germany, 2006; pp. 1–475.
34. Garcia Márquez, F.P.; Tobias, A.M.; Pérez, J.M.P.; Papaalias, M. Condition monitoring of wind turbines: Techniques and methods. *Renew. Energy* **2012**, *46*, 169–178. [[CrossRef](#)]
35. Sheng, S. NREL's Wind Turbine Drivetrain Condition Monitoring and Wind Plant Operation and Maintenance Research during the 2010s: A US Land-Based Perspective. *Acoust. Aust.* **2021**, *49*, 239–249. [[CrossRef](#)]
36. Lin, Y.; Tu, L.; Liu, H.; Li, W. Fault analysis of wind turbines in China. *Renew. Sustain. Energy Rev.* **2016**, *55*, 482–490. [[CrossRef](#)]
37. Abbaspour, A.; Mokhtari, S.; Sargolzaei, A.; Yen, K.K. A Survey on Active Fault-Tolerant Control Systems. *Electronics* **2020**, *9*, 1513. [[CrossRef](#)]

38. Edwards, C.; Spurgeon, S. *Sliding Mode Control: Theory and Applications*; CRC Press: London, UK, 1998. [\[CrossRef\]](#)
39. Olabi, A.G.; Wilberforce, T.; Elsaid, K.; Sayed, E.T.; Salameh, T.; Abdelkareem, M.A.; Baroutaji, A. A Review on Failure Modes of Wind Turbine Components. *Energies* **2021**, *14*, 5241. [\[CrossRef\]](#)

Disclaimer/Publisher's Note: The statements, opinions and data contained in all publications are solely those of the individual author(s) and contributor(s) and not of MDPI and/or the editor(s). MDPI and/or the editor(s) disclaim responsibility for any injury to people or property resulting from any ideas, methods, instructions or products referred to in the content.